Review of Scientific Instruments

RESEARCH ARTICLE | OCTOBER 02 2024

Determination of the response for the National Ignition Facility particle time of flight (PTOF) detector using single particle counting

Special Collection: Proceedings of the 25th Topical Conference on High-Temperature Plasma Diagnostics

Y. Lawrence ✉ ; B. L. Reichelt ; C. W. Wink ; G. Rigon ; M. Gatu Johnson ; C. K. Li ; J. A. Frenje

Check for updates

Rev. Sci. Instrum. 95, 103508 (2024)
https://doi.org/10.1063/5.0219541

View Online Export Citation

Articles You May Be Interested In

A magnetic particle time-of-flight (MagPTOF) diagnostic for measurements of shock- and compression-bang time at the NIF (invited)

Rev. Sci. Instrum. (July 2014)

Determining spectral response of the National Ignition Facility particle time of flight diagnostic to x rays

Rev. Sci. Instrum. (March 2023)

Learning from each other: Cross-cutting diagnostic development activities between magnetic and inertial confinement fusion (invited)

Rev. Sci. Instrum. (September 2024)

11 January 2025 19:21:37

MCL MAD CITY LABS INC.

Closed Loop Nanopositioning Systems with Picometer precision, Low noise and High stability

Force Microscopy and Single Molecule Microscopy Instruments for Quantum, Materials, and Bioscience

Custom Design and Innovative Solutions for the Nanoscale World

Think Nano® | Positioning | Microscopy | Solutions

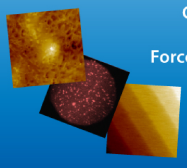

AIP Publishing

Review of Scientific Instruments ARTICLE pubs.aip.org/aip/rsi

Determination of the response for the National Ignition Facility particle time of flight (PTOF) detector using single particle counting

Cite as: Rev. Sci. Instrum. 95, 103508 (2024); doi: 10.1063/5.0219541
Submitted: 17 May 2024 • Accepted: 3 September 2024 •
Published Online: 2 October 2024

View Online Export Citation CrossMark

Y. Lawrence,[a] B. L. Reichelt, C. W. Wink, G. Rigon, M. Gatu Johnson, C. K. Li, and J. A. Frenje

AFFILIATIONS

Massachusetts Institute of Technology, Cambridge, Massachusetts 02139, USA

Note: This paper is part of the Special Topic on Proceedings of the 25th Topical Conference on High-Temperature Plasma Diagnostics.

[a]**Author to whom correspondence should be addressed:** ylaw@mit.edu

ABSTRACT

The Particle Time of Flight (PTOF) detector is a chemical vapor deposition diamond-based detector used to measure bang times in low-yield ($\lesssim 10^{15}$ neutrons) experiments at the National Ignition Facility (NIF) at Lawrence Livermore National Laboratory (LLNL). Historically, the impulse response for PTOF diamond detectors has been obtained from x-ray timing shots on the NIF and shots on the MegaRay pulsed electron accelerator at LLNL. The impulse response may alternatively be obtained using single particle interactions with the detector, at substantially less cost and higher frequency compared to NIF timing shots, which typically occur months apart. Here, the response of a PTOF detector setup is characterized by statistically averaging a large number of single particle waveforms. A high fidelity instrument response function can be constructed in this way. This is confirmed by comparison of the single particle counting-constructed response to the impulse response function measured for the same detector at LLNL's MegaRay facility.

© 2024 Author(s). All article content, except where otherwise noted, is licensed under a Creative Commons Attribution (CC BY) license (https://creativecommons.org/licenses/by/4.0/). https://doi.org/10.1063/5.0219541

11 January 2025 19:21:37

I. INTRODUCTION

The Particle Time of Flight (PTOF) detector is used on the National Ignition Facility[1] (NIF) to measure bang times on low-yield ($\lesssim 10^{15}$ neutrons) shots for a variety of particle types, including x rays and deuterium–tritium (DT)-neutrons, DD-neutrons, and D^3He-protons, from the following fusion reactions:[2]

$$D + T \rightarrow \alpha\,(3.5\,\mathrm{MeV}) + n\,(14.1\,\mathrm{MeV}), \quad (1)$$

$$D + D \rightarrow {}^3He\,(0.82\,\mathrm{MeV}) + n\,(2.45\,\mathrm{MeV}), \quad (2)$$

$$D + {}^3He \rightarrow \alpha\,(3.6\,\mathrm{MeV}) + p\,(14.7\,\mathrm{MeV}). \quad (3)$$

If the burn duration is long enough compared to the detector rise time, PTOF is also capable of measuring burn histories.[3] The PTOF detector consists of a chemical vapor deposition (CVD) diamond coated with several thin metallic layers (see Sec. V for more details) and seated inside of a brass assembly. Microwave assisted chemical vapor deposition is used to grow PTOF diamonds and involves injecting gases into a reaction chamber and ionizing them into a plasma, leading to high purity deposition of carbon atoms onto a substrate.[4] The diamonds used for PTOF detectors are supplied by Applied Diamond and Diamond Materials GmbH. The diameters and thicknesses of the diamonds used for PTOF range from 2 to 10 mm and 0.2 to 1 mm, respectively, and their nitrogen impurity content is < 1 ppm. Historically, polycrystalline diamonds were used, but more recently, single crystal diamonds are being used in PTOF detectors to take advantage of their usually shorter rise times. A bias voltage (typically 500 V) is applied to the diamond to sweep the charges of electron–hole pairs excited by incident radiation. This induces a current, which is recorded as a voltage signal on an oscilloscope.

To extract a bang time measurement from a NIF shot, a forward fitting procedure is carried out. This involves convolving an emission history (usually assumed to be a Gaussian profile in time) with the detector impulse response function (IRF) and the time of

© Author(s) 2024

flight impulse response to obtain a fit to the measured voltage signal. Using a gradient descent algorithm, the bang time is varied until the best fit of the model to the data is obtained.

To carry out this forward fit procedure and obtain an accurate bang time measurement, the IRF of the given PTOF detector must be well characterized. Historically, PTOF detector IRFs have been obtained from x-ray timing shots using the Advanced Radiographic Capability[5] (ARC) at NIF, which produces 10 ps pulses of ~MeV x-rays. IRFs have also been obtained from the MegaRay Facility at Lawrence Livermore National Laboratory (LLNL).[3] MegaRay is a 10 Hz, 30 MeV electron accelerator that provides 5 ps pulses of electron bunches. These electron bunches can impinge directly on the PTOF detector (direct case), or a Ta foil (575–1000 μm thickness) can optionally be placed in front of the PTOF detector, itself situated off-axis from the electron beam, to lower the fluence on the detector and provide x-rays via bremsstrahlung emission (indirect case), although Geant4[6] simulations have shown that the majority of the deposited energy in this indirect setup is still due to electrons.[3] For the same diamond and voltage bias, averaged IRFs from the direct and indirect setups generally agree in the rise times, but the direct setup generally leads to longer fall times. MegaRay IRFs, when convolved with a cable chain model corresponding to the NIF cable chain, have been found to be in good agreement with IRFs obtained from ARC timing shots.[3]

The major drawback of these impulse sources is their operational complexity and low, scheduling-inhibited frequency with which to obtain IRFs for PTOF detectors. This delays repeat measurements of detector IRFs to ensure IRF repeatability, as well as the usage of new PTOF detectors until their IRFs can be well characterized on either of these two radiation sources. Single particle counting with a small 0.13 μCi radiation source and benchtop testing equipment is a significantly cheaper alternative, which enables much more frequent acquisition of PTOF detector IRFs. Single particle counting can provide well characterized, averaged IRF measurements, as has been performed for neutron time-of-flight detectors.[7] In this article, we describe this procedure and demonstrate the viability of this technique for obtaining well-characterized PTOF IRFs by comparing to IRFs previously obtained at MegaRay.

II. SINGLE PARTICLE COUNTING TESTING SETUP

To obtain an IRF from single particle interactions with the detector, a benchtop PTOF testing setup is employed. The cable chain consists of the PTOF detector, which transmits signal to a Picosecond Pulse Labs Model 5531 bias tee and Model 5840B-107 21 dB amplifier, and the voltage traces are recorded on a 6 GHz, 25 GSa/s Tektronix DPO70604C oscilloscope. A bias voltage of −500 V is applied to the PTOF diamond. The diamond used for this study has a diameter of 1 cm and a thickness of 1 mm.

Cosmic background radiation as well as a 0.13 μCi Ra226 source are used to provide a single event signal in the detector. The decay of Ra226, as well as its decay products, release α particles primarily at five different energies: 4.78, 5.30, 5.49, 6.00, and 7.69 MeV.[8] For the Ra226 source case, the source is simply placed on top of the detector, with a 1.5 mm separation between the source and the front surface of the detector. For the cosmic background case, the Ra226 source is removed, while the rest of the setup remains the same. For the Ra226 source case, waveforms due to cosmic rays are still measured. For this test case, for which particles both from the Ra226 source and the cosmic background are detected, a voltage peak threshold of 0.05 V is applied to discriminate against measured waveforms from cosmic background radiation.

III. SINGLE PARTICLE WAVEFORMS

Single particle waveforms were collected for both test cases with and without the Ra226 source, the latter measuring only cosmic background radiation. Approximate count rates are 0.05 Hz for the Ra226 source case and 0.02 Hz for the cosmic background case. The latter is similar to the expected count rate of 0.79 min^{-1} due to the muon flux at Earth's surface (~1 muon/cm^2/min),[9] given the detector surface area of 0.79 cm^2. Raw, unnormalized waveforms are shown in Fig. 1. The peak voltage for the cosmic background case is 0.04 ± 0.03 V. Waveforms with similar peak voltage are measured with the Ra226 source, but significantly higher voltage waveforms are also measured. Excluding those waveforms with a peak voltage less than 0.05 V, which are taken to be due to cosmic background, the average value of the peak voltage for the Ra226 source case is 0.13 ± 0.02 V. Henceforth, we use the same peak voltage threshold of 0.05 V to discard cosmic background impulses from Ra226 source impulses when characterizing IRFs for both cases.

Normalizing these raw waveforms to their peak voltage values and averaging them for each test case (i.e., at each time, taking the average of the signal values from all the normalized waveforms for the given case), we obtain IRFs for cosmic background particles and Ra226 source particles, as shown in Fig. 2. Errors are calculated as the standard deviation of signal values of the given case's waveforms at a given time.

These IRFs are characterized by rise and fall times (20%–80% percent of peak voltage, and vice versa, respectively) as presented in Table I. Full width at half maximum (FWHM) values are also provided for each case.

The waveforms for each case were interpolated to obtain more accurate rise and fall times than would be obtained otherwise, given the relatively low sampling rate of the oscilloscope on the rising edge.

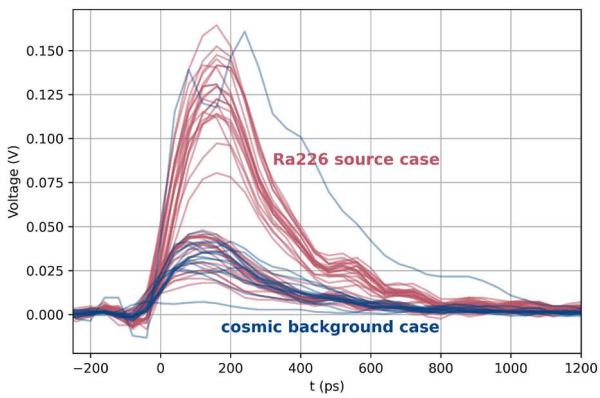

FIG. 1. Raw measured waveforms due to single particle counts for the Ra226 source and cosmic background test cases. Note that the Ra226 source case data still include waveforms due to cosmic background radiation, as indicated by those waveforms with a similar voltage peak as most of the cosmic background waveforms, for which the average peak voltage is 0.04 ± 0.03 V.

11 January 2025 19:21:37

© Author(s) 2024

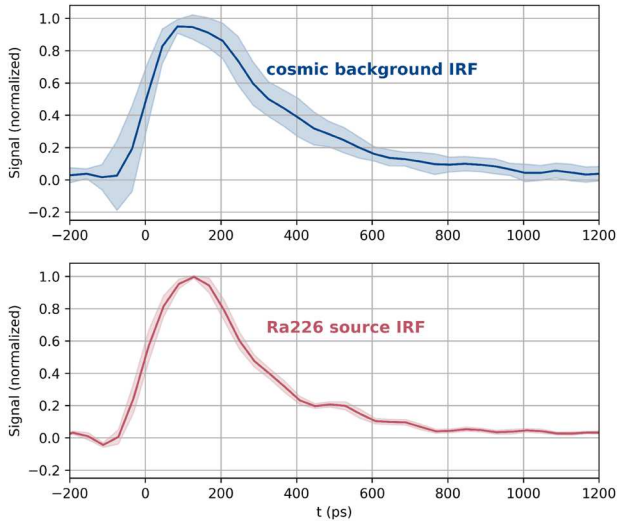

FIG. 2. Normalized IRFs for the cosmic background and Ra226 source cases.

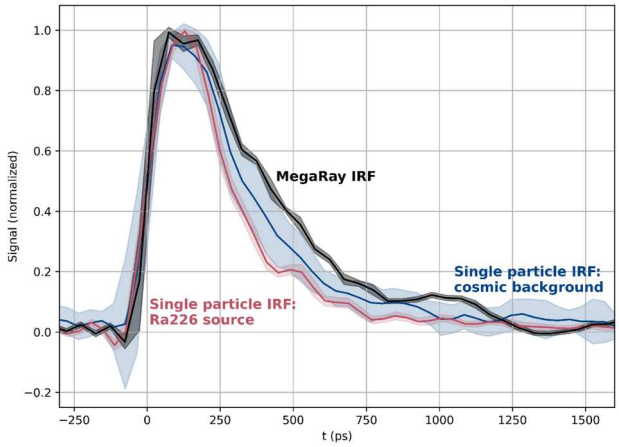

FIG. 3. Comparison between single particle IRFs (cosmic background and Ra226 source) and the IRF obtained for the same PTOF diamond at the MegaRay electron accelerator. Shaded regions indicate one standard deviation about the mean of the averaged IRF.

The waveforms were interpolated at ≈2 TSa/s (100× the oscilloscope sampling rate) using cubic splines; using a linear interpolation and/or slightly different sampling rates for the interpolation do not appreciably affect the results. Rise and fall times, as shown in Table I, were obtained by averaging the rise and fall times of all the interpolated waveforms for a given case. The same procedure was carried out for the FWHM values in Table I. The single particle IRFs (cosmic background and Ra226 source cases) have similar rise times and fall times to within error.

IV. COMPARISON TO MEGARAY IRF

Experiments at LLNL's MegaRay Facility were previously conducted to obtain well-characterized IRFs for several CVD diamonds. To assess the viability of using IRFs obtained from single particle counts in Sec. II, the IRFs for the Ra226 source and cosmic background cases are compared to the IRF obtained for the same PTOF diamond at MegaRay. The MegaRay waveforms are produced by electron bunches, and typical measured peak voltages for the MegaRay runs with the same diamond are ~1 V, ten times higher than those of the Ra226 source single particle waveforms. In addition, a Keysight DSO-S 804A 8 GHz, 20 GSa/s oscilloscope along with 20 dBW of attenuation was used at MegaRay as opposed to the 6 GHz oscilloscope and 21 dB, 13.5 GHz amplifier as utilized in Secs. II and III.

The IRFs for all three cases are plotted in Fig. 3. The rise and fall times of the MegaRay IRF, found in the same manner as the single particle IRFs, are also presented in Table I. All three IRFs exhibit similar shapes. However, the MegaRay IRF has a significantly shorter rise time and longer fall time compared to the single particle IRFs. This could be caused by the different types of radiation used to generate each IRF, in particular, 30 MeV electron bunches for the MegaRay IRF and a few MeV α particles for the single particle IRF for the Ra226 source case. Electron scattering in the diamond could contribute to a longer fall time for the MegaRay IRF.

In addition, the single particle IRFs may have larger rise times because of the smaller, 6 GHz bandwidth on the oscilloscope used to collect those waveforms vs 8 GHz at MegaRay. These bandwidths equate to 20%–80% oscilloscope rise times of 37 and 28 ps, respectively. In addition, there is the signal broadening introduced by the 13.5 GHz amplifier, corresponding to a rise time of 16 ps.

While there are statistically significant discrepancies between the three IRFs, most features of interest in PTOF signals (primarily burn widths, typically on the order of[3] ~200 ps) are wider than these IRFs' rise times. Therefore, the forward fitting procedure (see Sec. I) used to analyze PTOF traces will generally yield similar results in terms of bang times (and possibly burn histories) across these three average IRFs.

TABLE I. Summary of IRF parameters.

Case	Event rate (Hz)	Rise time (ps)	Fall time (ps)	FWHM (ps)
Cosmic background (i.e., No. Ra226 source)	≈0.02	70 ± 30	330 ± 50	330 ± 60
Ra226 source	≈0.05	80 ± 4	240 ± 40	278 ± 9
MegaRay	10	46 ± 2	406 ± 6	411 ± 4

11 January 2025 19:21:37

© Author(s) 2024

V. EXPECTED SINGLE PARTICLE RESPONSE

While the cosmic background provides measurable single particle counts, it is preferable to obtain IRFs specifically from the Ra226 source because its decay particles and energies are well known. To help verify the particle type being detected in the single particle waveforms, the expected single particle response of the PTOF detector was analyzed. This analysis was also performed to understand the discrepancy between the expected count rate ($\gg 1$ counts/s) and the measured count rate with the Ra226 source (~0.05 counts/s).

A TRIM[10] simulation was carried out to calculate the straggling of incident α particles from the Ra226 source into the PTOF detector. The layers of material traversed include a 1.5 mm air gap, several thin metallic coatings (1 μm of Au, 200 nm of Pt, and 200 nm of Ti), and the diamond layer itself, which constitutes the active detection medium. The α particle energy spectrum at the diamond surface (i.e., at the Ti–diamond interface) is given in Fig. 4, which shows that stopping incident α particles before reaching the diamond is expected to be significant but not sufficient to range them out prior to the diamond detection medium. Starting from the given birth energy, the incident α particles are downranged by ~750 keV by the air and thin metallic layers and expected to deposit their remaining $\gtrsim$4 MeV energy within the diamond, with a range of 10 s of μm. α particle energies at the diamond surface, corresponding to the five birth energies, are calculated to be 4.00, 4.57, 4.76, 5.32, and 7.09 MeV, all with FWHM = 0.06 MeV. Most of the stopping before reaching the diamond occurs in the thin metallic layers of Au, Pt, and Ti, rather than the air gap. In addition, separate testing was carried out with a different diamond detector (Cividec A30027 Diamond Fast-Neutron Monitor consisting of B70064 Fast-Neutron Diamond Detectors (single crystal, 500 μm thick, impurity content of $\lesssim$ 1 ppb) and CxL0220 Spectroscopic Amplifier), which verified that the Ra226 source emission rate is $\gg 1$ s^{-1} as expected, as this high count rate was measured on this different diamond detector. These tests were conducted with various combinations of diamonds and amplifiers, using the same oscilloscope (6 GHz, 25 GSa/s), indicating that the diamond detector discussed throughout this article is the cause of the unexpectedly low count rate.

The stopping calculations indicate that α particles are expected to be the dominant source of counts with a count rate $\gg 1$ s^{-1}. However, the measured single particle count rate (~0.05 counts/s) differs by orders of magnitude.

To assess this discrepancy, the expected deposited charge was compared with the averaged measured charge, $Q_{measured}$, given the voltage traces from the Ra226 source case and 21 dB amplification. The expected deposited charge is[11] $Q_{expected} = e(E_\alpha/\epsilon)(d/D) = e(E_\alpha/\epsilon)(\mu E\tau/D)$, where e is the electron charge, E_α is the incident α energy from the Ra226 source, $\epsilon = 13$ eV is the excitation energy for diamond, $d = \mu E\tau$ is the recombination distance, $D = 1$ mm is the diamond thickness, μ is the average carrier mobility, E is the electric field strength in the diamond, and τ is the charge carrier lifetime before recombination. Setting $Q_{measured} = Q_{expected}$ and choosing $E_\alpha = 5$ MeV as a rough average of deposited α particle energy, the recombination distance, expected to be $d < D$, is instead inferred to be $d \approx 1.4$ mm > 1 mm $= D$. This value is significantly larger than the expected value of $d \sim 1 - 50$ μm, using the known electric field strength, carrier lifetime estimated from the falling edge exponential decay time constant ($\tau \sim 300$ ps as a rough average from the three IRFs shown in Fig. 3), and the mobility calculated from MegaRay experiments[3] ($\mu \sim 75$ cm^2/V s) and for pure diamond[12] ($\mu = 3200$ cm^2/V s) for the lower and upper ends, respectively, of the estimate. This may point to a different particle type being detected, although the higher count rate and peak voltages for the Ra226 source case compared to the cosmic background case make this unlikely. Considering α particles then, the inferred recombination distance being on the order of or larger than the diamond thickness suggests that the diamond excitation energy is lower than assumed, perhaps due to the presence of charge in localized shallow traps with a much lower ionization energy than the full diamond bandgap.

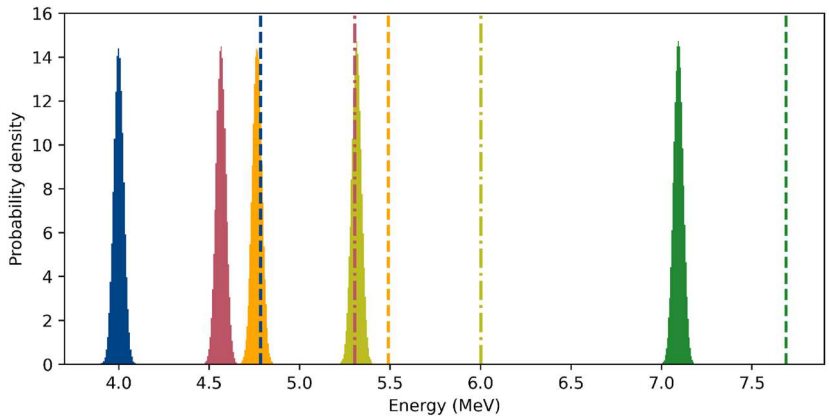

FIG. 4. Energy spectrum of α particles from Ra226 source at diamond surface from TRIM straggling simulation. Dashed lines indicate birth energies of 4.78, 5.30, 5.49, 6.00, and 7.69 MeV for the corresponding peaks with the same colors. The corresponding energies at the diamond surface are, respectively, 4.00, 4.57, 4.76, 5.32, and 7.09 MeV, all with FWHM = 0.06 MeV. Probability densities are plotted for each peak separately.

11 January 2025 19:21:37

© Author(s) 2024

A proposed explanation for the unexpectedly low count rate of α particles for the Ra226 source case is the presence of isolated, spatially localized impurity centers. It is hypothesized that charge carrier production is higher when such regions of the lattice are struck by incident α particles, compared to pure regions of the diamond, for which the charge carrier production may be too low to produce a signal above the noise floor on the oscilloscope. Defect trapping may lead to a higher noise floor via more leakage in the PTOF diamonds that were tested. In contrast, reduced defect trapping in the single crystal, ~10× purer Cividec diamond discussed earlier may explain its much higher count rate, as the signal amplitude on these events was small (on the order of the oscilloscope noise floor when using the PTOF diamond), such that these events may have been too weak to be detected on the PTOF diamond (except for the relatively rare presence of spatially localized impurity centers producing signals above the noise floor).

VI. CONCLUSION

IRFs of a PTOF detector were obtained using single particle counts on a benchtop testing setup and found to be similar to the IRF for the same detector, obtained at the MegaRay electron accelerator. These results demonstrate the viability of obtaining PTOF IRFs through single particle counting.

Future work will apply this technique to characterize the impulse responses for more PTOF detectors, as well as using more radiation sources, including Am241. Furthermore, the cause of the discrepancy between the measured count rate and the expected count rate will be determined through further characterization of the PTOF diamonds as well as more single particle testing, such as selective particle filtering to rule out counts due to certain particle types.

ACKNOWLEDGMENTS

The authors acknowledge John Ball, Shon Mackie, and Roy Tinguely for assistance in troubleshooting the diamond detector and other cable chain components. This work was supported, in part, by the U.S. Department of Energy NNSA MIT Center-of-Excellence under Contract No. DE-NA0003868 and by LLNL under Contract No. B656484. This report was prepared as an account of work sponsored by an agency of the United States Government. Neither the United States Government nor any agency thereof, nor any of their employees, makes any warranty, express or implied, or assumes any legal liability or responsibility for the accuracy, completeness, or usefulness of any information, apparatus, product, or process disclosed, or represents that its use would not infringe privately owned rights. Reference herein to any specific commercial product, process, or service by trade name, trademark, manufacturer, or otherwise does not necessarily constitute or imply its endorsement, recommendation, or favoring by the United States Government or any agency thereof. The views and opinions of authors expressed herein do not necessarily state or reflect those of the United States Government or any agency thereof.

AUTHOR DECLARATIONS

Conflict of Interest

The authors have no conflicts to disclose.

Author Contributions

Y. Lawrence: Data curation (equal); Formal analysis (lead); Writing – original draft (lead); Writing – review & editing (equal). **B. L. Reichelt**: Conceptualization (equal); Data curation (equal); Formal analysis (supporting); Investigation (supporting); Writing – review & editing (equal). **C. W. Wink**: Data curation (supporting); Investigation (supporting); Writing – review & editing (supporting). **G. Rigon**: Data curation (supporting); Investigation (supporting). **M. Gatu Johnson**: Conceptualization (equal); Funding acquisition (equal); Project administration (equal); Supervision (lead); Writing – review & editing (equal). **C. K. Li**: Funding acquisition (equal); Project administration (equal). **J. A. Frenje**: Funding acquisition (equal); Project administration (equal).

DATA AVAILABILITY

The data that support the findings of this study are available from the corresponding author upon reasonable request.

REFERENCES

[1] S. W. Haan *et al.*, Phys. Plasmas **18**, 051001 (2011).
[2] H. G. Rinderknecht *et al.*, Rev. Sci. Instrum. **83**, 10D902 (2012).
[3] B. Reichelt, R. Kishimori, Y. Lawrence, C. Wink, M. Johnson, T. Johnson, K. Hahn, R. Marsh, M. Eckart, D. Gibson, E. Mariscal, M. Rubery, K. Meany, H. Geppert-Kleinrath, J. Kunimune, P. Adrian, K. Baker, D. Casey, S. Dannhoff, T. Evans, D. Higginson, N. Izumi, N. Kabadi, S. Kerr, O. Landen, D. Martinez, J. Pearcy, R. Petrasso, D. Rusby, L. Russell, D. Schlossberg, V. Smalyuk, R. Tommasini, J. Frenje, and C. Li, "Ultra-fast single-crystal CVD diamonds in the Particle Time-Of-Flight (PTOF) detector for low yield burn-history measurements on the NIF," Rev. Sci. Instrum. (submitted) (2024).
[4] L. Sun, G. Yuan, L. Gao, J. Yang, M. Chhowalla, M. H. Gharahcheshmeh, K. K. Gleason, Y. S. Choi, B. H. Hong, and Z. Liu, Nat. Rev. Methods Primers **1**, 5 (2021).
[5] J. Di Nicola, S. Yang, C. Boley, J. K. Crane, J. Heebner, T. M. Spinka, P. Arnold, C. Barty, M. Bowers, T. Budge *et al.*, Proc. SPIE **9345**, 93450I (2015).
[6] S. Agostinelli, J. Allison, K. a. Amako, J. Apostolakis, H. Araujo, P. Arce, M. Asai, D. Axen, S. Banerjee, G. Barrand *et al.*, Nucl. Instrum. Methods Phys. Res., Sect. A **506**, 250 (2003).
[7] J. D. Styron, C. Ruiz, K. Hahn, G. Cooper, G. Chandler, B. Jones, B. McWatters, C. Forrest, J. Vaughan, J. Torres *et al.*, Rev. Sci. Instrum. **89**, 10I119 (2018).
[8] C. Nebelung and L. Baraniak, Appl. Radiat. Isot. **65**, 209 (2007).
[9] H. Gadey, S. Chatzidakis, and A. T. Farsoni, Appl. Radiat. Isot. **163**, 109209 (2020).
[10] J. F. Ziegler and J. P. Biersack, in *Treatise on Heavy-Ion Science: Volume 6: Astrophysics, Chemistry, and Condensed Matter* (Springer, 1985), pp. 93–129.
[11] T. Behnke, P. Hüntemeyer, A. Oh, J. Steuerer, A. Wagner, and W. Zeuner, Nucl. Instrum. Methods Phys. Res., Sect. A **414**, 340 (1998).
[12] L. S. Pan, D. Kania, P. Pianetta, J. Ager III, M. Landstrass, and S. Han, J. Appl. Phys. **73**, 2888 (1993).

11 January 2025 19:21:37

© Author(s) 2024